Switchable Chiroptical Hot-Spots in Silicon Nanodisk Dimers

Xin Zhao and Björn M. Reinhard*

Department of Chemistry and The Photonics Center, Boston University, Boston, MA 02215, United States

*E-mail: bmr@bu.edu

Abstract: We demonstrate uniform sign optical chirality generation in dimers of silicon (Si) nanodisks under linear light polarization through combination of experimental spectroscopy and electromagnetic simulations. Excitation of the magnetic dipole resonance in individual Si nanodisks generates enhanced electric and magnetic fields. We show that the fields provided by adjacent Si nanodisks excited with linearly polarized light at the magnetic dipole resonance can align to generate strong near-field chirality in the gap between the Si nanodisks. The near-field chirality enhancement for Si nanodisk dimers is compared with that for resonant gold (Au) nanoparticle dimers that provide almost exclusively electric field enhancement. We experimentally determine the third Stokes parameter, S_3, of light transmitted through Si nanodisk dimers fabricated on sapphire as a measure for the chirality flux and the related near-field chirality. The experiments confirm the generation of uniform sign optical chirality in the Si nanodisk dimers whose handedness can be switched through choice of the orientation of the incident linear light polarization and whose amplitude decreases with increasing gap separation.

Key words: silicon, magnetic dipole, optical chirality, chirality flux, stokes parameter

Chirality is a fundamental aspect of stereochemistry and light-matter interactions. Chiral molecules exist in two enantiomers, which are mirror images of each other that cannot be superimposed through translation or rotation and are said to have different “handedness”. The chirality of molecules or of specific stereocenters within larger molecules impacts the interactions of these molecules with light, and the resulting optical activity (OA) results in a rotation of an incident linear light polarization.[1] Molecules that rotate clockwise are referred to as the D-form, whereas molecules that rotate the light anti-clockwise are the L-form. Intriguingly, for many biological molecules, including the elementary building blocks of all proteins, the amino acids, one enantiomer is prevalent in living systems. As chirality plays an important role in the functionality of biomolecules,[2,3] assays capable of detecting and discriminating different chiral stereoisomers, ideally with small sample quantities and at low concentration are necessary. The concept of chirality is not limited to molecules but also applies to electromagnetic fields.[4] Circularly polarized light (CPL) is chiral and exists in two handednesses, left and right CPL, that interact differently with chiral stereoisomers. Electronic[5] and vibrational[6] circular dichroism (CD) spectroscopy utilizes differences in the relative absorption of optically active molecules when excited by CPL of defined handedness to detect and characterize molecular chirality.[7] CD signal intensities are, however, intrinsically weak and require relatively large sample quantities. This drawback is well recognized, and there has recently been tremendous interest in the development of electromagnetic materials that enhance chiral light-matter interactions to alleviate the detection and identification of chiral stereoisomers.

The difference in absorption of a monochromatic CPL plane wave at a frequency ω by a chiral molecule is directly proportional to the optical chirality density, given as $C = -\frac{\varepsilon_0 \omega}{2} Im(\boldsymbol{E}^* \cdot \boldsymbol{B})$.[8] $\boldsymbol{E}$ and $\boldsymbol{B}$ are the complex electric and magnetic field, respectively. The magnetic field is related to the magnetic field strength, $\boldsymbol{H}$ *via* the permeability, μ: $\boldsymbol{B} = \mu\boldsymbol{H}$. From this analysis it follows that

CD signals can be enhanced by boosting *C* through a parallel alignment of electric and magnetic field components that are not in phase. For detection of one specific handedness a uniform sign enhancement of *C* is desirable, and significant efforts have been undertaken in the field of plasmonics to achieve a uniform sign enhancement of *C* with custom-designed plasmonic nanostructures.[7,9–19] Initially these designs were based on nanostructures that were by themselves chiral, but difficulties in subtracting weak molecular signal from strong plasmonic resonances led to the development of achiral antennas that still fulfill the requirements of uniform-sign *C* generation.[9,20–22] Intriguingly, Tian *et al.* predicted through electromagnetic simulations that dimers of gold (Au) nanoparticles can generate a uniform-sign *C* "hot-spot" even under linearly polarized light polarization at the plasmon resonance frequency of the dimer.[9] The generation of enhanced optical chirality in an achiral antenna with linearly polarized light paves the path to characterizing molecular chirality at low concentrations without the need for CPL, which is of high general and practical relevance.

Silicon (Si) nanoparticles have recently attracted considerable attention as alternative to metallic nanoparticles as elementary building blocks for nanoantennas and meta-surfaces.[23–28] Si nanoparticles, unlike metal nanoparticles, support both electric as well as magnetic Mie resonances of significant strength in the visible range of the electromagnetic spectrum.[29–36] These resonances arise from charge displacements in the high refractive index material. For Si nanodisks the magnetic and electric dipole resonances are almost independently tunable *via* the aspect ratio of the nanodisks.[34,36,37] Solomon *et al.* investigated the near-field chirality enhancement in Si nanodisks with spectrally overlapping magnetic and electric dipole resonances through 3-dimensional full field electromagnetic simulations under CPL illumination.[38] The authors demonstrated that spatially overlapping and enhanced ***E***- and ***H***- fields with a phase shift of $\pi/2$ provided by the high refractive index nanodisks generate a strong enhancement of *C*. Discrete assemblies of Si nanoparticles, such as a gap-separated dimers,[31,39–42] rovide additional degrees

of freedom for enhancing and aligning electromagnetic fields and boosting the near-field chirality in the ambient medium through interactions of the evanescent fields generated by the individual building blocks. Importantly, different from dimers of metallic nanoparticles, for which only the ***E***-fields hybridize to generate increased ***E***-field intensity in the gap between the nanoparticles,[43–46] for dimers of Si nanoparticles ***E***-***E***, ***H***-***H*** and ***E***-***H*** field interactions are feasible, resulting in a localization and enhancement of both ***E***- and ***H***-fields in the interparticle gap region.[31,47] The availability of both enhanced ***E***- and ***H***-fields at one given wavelength makes Si nanodisks unique building blocks of achiral antennas that create regions of enhanced near-field chirality in the ambient medium. Yao and Li have performed simulations to investigate the formation of chiral hot spots in discrete dimers of silicon nanocubes when excited with CPL through electromagnetic simulations.[41] In this paper we will demonstrate that discrete dimers of Si nanoparticles provide opportunities for generating chiral hot spots even for excitation with linearly polarized light. We focus our analysis in this work on dimers of silicon nanodisks as these nanostructures are easy to generate with conventional fabrication techniques and, thus, make the concept experimentally tractable through measurements of the optical chirality flux. Another important component of our analysis in this manuscript is an explicit comparison with dimers of Au nanodisks. Although the excitation of the localized surface plasmon resonance (LSPR) in noble metal nanoparticles provides higher ***E***-field intensities than is possible in Si nanodisks, *C* enhancement in the metal NP dimer relies on interactions of the enhanced ***E***-field with the very weak incident ***H***-field.[9,48,49] The hypothesis to be tested in this work is that the enhancement of both ***E***- and ***H***-fields in dimers of Si nanoparticles at the magnetic dipole resonance can compensate a weaker peak ***E***-field enhancement when compared with resonant noble metal nanoparticle dimers at the same wavelength and still result in a comparable if not stronger *C* enhancement. To address this question, we characterize the evolution of the same-sign near-field chirality in symmetric Si nanodisk dimers when excited through linearly polarized light through electromagnetic

simulations and optical spectroscopy. We compare the gap width dependence of the chirality density in high refractive index Si nanodisk dimers with that of plasmonic Au nanodisk dimers and experimentally validate the creation of switchable chiroptical hot-spots in Si nanodisk dimers by far-field measurements of the optical chirality flux.

Methods

Simulations: Numerical electromagnetic analyses were carried out by finite difference time domain (FDTD) (Lumerical Solution Inc.) simulations. Scattering spectra were simulated by applying a total field scattered field (TFSF) source as the incident light with the wave vector (*k*) pointing in the z direction. A fine mesh with maximum mesh size of λ/80 was used. Perfectly matched layer (PML) boundary condition (BC) was imposed on all planes. The scattered light intensity was calculated by integrating the power transmitted through a box monitor surrounding the structure. For near-field simulations, a plane wave was used as incident light with periodic BC imposed on x and y planes and PML BC on z planes. A fine mesh with a mesh size of 2-5 nm was used (depending on the gap size) to ensure enough resolution in the gap area. The near-field data was extracted from a xy-plane monitor located in the midplane of the respective structures.

Fabrication: The Si on sapphire (SoS) substrate (UniversityWafer, Inc.) with Si EPI layer of 230 nm +/- 10 nm on top of monocrystalline Al_2O_3 base was first treated with piranha solution to remove organic residues off the substrate for further fabrication. Designed nanodimer arrays were then patterned through electron beam lithography (EBL) by Zeiss SUPRA 40VP SEM on A3 poly (methyl methacrylate) (PMMA) spin-coated substrate. A 60 nm aluminum layer was then evaporated onto the developed substrate using electron beam evaporation (CHA Industries, Fermon, CA, U.S.A) to serve as the protective layer for the following reactive ion etching (RIE) step. An inductively coupled plasma reactive ion etching (ICP-RIE, STS company) was used with

a gas mixture of SF_6/C_4F_8 (60 / 155 sccm) at a forwarding power of 1050 W for ~1 min to generate Si nanodimer arrays with a final height of approximately 230 nm. After removing the Al layer by Al etchant Type A, the sample was subjected to RIE using the same conditions to reach a final height of ~150 nm. Dummy samples were used every time before the final etching to control the etching time and the final heights of the samples were determined using a profilometer.

Experimental Characterization: Experimental transmission data was collected with an upright microscope. The incident broadband light passed through a linear polarizer before it hits the sample. The transmitted light was then collected by a low NA (NA = 0.3) 20x objective. To detect transmitted light with a specific handedness, an analyzer consisting of a quarter-wave plate and a linear polarizer was positioned in the detection channel with the linear polarizer aligned precisely $\pm\pi/4$ to the quarter-wave plate optical axis.

Results

Electromagnetic Analysis of Achiral Si Nanodisk Dimers that Enhance the Near-Field Chirality, *C.* Monocrystalline Si nanodisks are experimentally easily accessible through reactive ion etching. [50,51] This fabrication approach also allows fabrication of nanodisk dimers of defined size and separation down to 20 nm with high accuracy. Similar as spherical nanoparticles, nanodisks provide electric and magnetic dipole resonances whose spectral position can be tuned across a broad spectral range though choice of their height and diameter.[30,52–54] **Figure 1a** shows the simulated scattering spectrum of a Si nanodisk with a height of h = 100 nm and diameter of D = 140 nm excited by a linearly polarized plane wave. Experimental scattering spectra are provided in **Figure S1a** of the Supporting Information. The electric dipole in the simulated spectrum at 496 nm results from the oscillation of the dielectric polarization along the incident ***E***-field vector, while the magnetic dipole resonance at 563 nm arises from an ***E***-field induced circular displacement

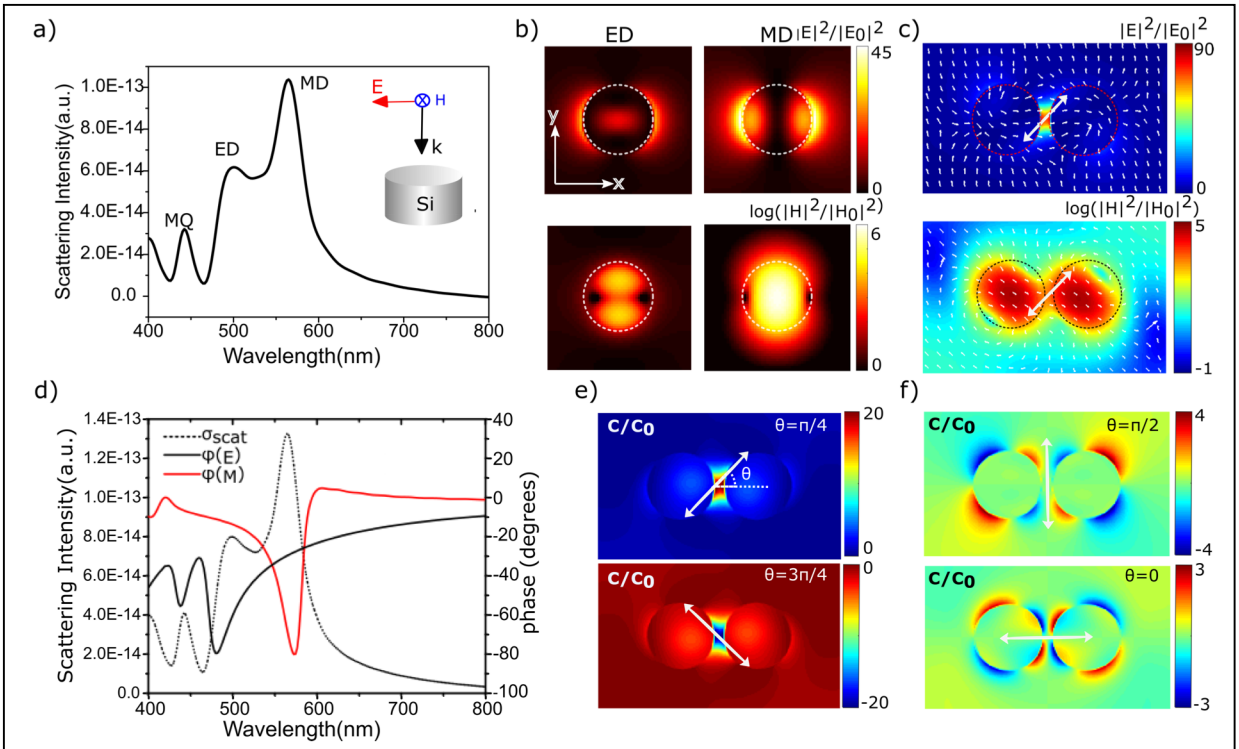

Figure 1: a) Simulated scattering spectrum of a free-standing silicon nanodisk monomer with a diameter of *D* = 140 nm and height of *h* = 100 nm under normal incidence. The peaks at 496 and 563 nm correspond to electric (ED) and magnetic (MD) dipole modes, respectively. b) ***E***- and ***H***-field intensity maps (xy-plane) for electric and magnetic dipole modes in the monomer. c) Normalized ***E***- (top) and ***H***- (bottom) field intensity maps (xy cross-section) for dimers of nanodisks with separation (edge-to-edge) of *g* = 20 nm at λ = 579 nm. Small white arrows show the vector fields. The orientation of the incident linear light polarization is given by the double-headed arrow. d) Simulated phase of E_x and H_x field components at a spot located on the xy diagonal at a height of 50 nm and a distance of 10 nm from a *D* = 140 nm and *h* = 100 nm Si nanodisk excited with ($\theta = \pi/4$). The simulated scattering spectrum (dotted line) is included for completeness. e-f) Simulated optical chirality enhancement for silicon nanodisk dimers (*D* = 140 nm, *h* = 100 nm, *g* = 20 nm) at λ = 579 nm with (e) off-axis polarization of the incident light ($\theta = \pi/4, 3\pi/4$) or (f) polarization pointing along ($\theta = 0$) or perpendicular ($\theta = \pi$) to the long dimer axis as control.

current. A weaker third peak is observed at around 442 nm, which is attributed to the magnetic quadrupole (MQ) resonance. The simulated ***E***- and ***H***-field intensity maps in the xy- plane calculated at the resonance frequencies of the electric and magnetic dipoles in **Figure 1b** show i.) that the magnetic and electric dipole resonances each enhance both ***E***- and ***H***-field intensities, ii.) that the ***E***- and ***H***-fields associated with one dipole resonance lie along orthogonal directions, and iii.) that the ***E***- and ***H***-fields of the magnetic dipole are stronger and penetrate deeper into the ambient medium than those of the electric dipole resonance. Especially the ***H***-field of the electric

dipole is almost completely confined to the interior of the nanodisk. The availability of increased ***E***- and ***H***-field intensities outside of the nanodisk at the magnetic dipole resonance facilitate strong electromagnetic interactions between Si nanodisks and forms the basis for a rational enhancement of the near-field chirality in discrete nanoparticle assemblies.

Although the ***E***- and ***H***-fields of the magnetic dipoles are orthogonal for individual nanodisks, in dimers anisotropic electromagnetic interactions between the nanoparticles achieve a colocalization of enhanced ***E***- and ***H***-fields in the gap for off-axis incident polarizations. For instance, a linearly-polarized ***E***-field (normal incidence) with a wavelength corresponding to the magnetic dipole resonance and an orientation of $\theta = \pi/4$ relative to the long dimer axis induces ***H***-fields pointing at an angle of ¾ π in both nanodisks (**Figure 1c,** bottom). As the induced magnetic fields around the individual nanodisks have a component parallel to the long dimer axis, the dipole resonances can couple and achieve a localization of enhanced ***H***-field intensity in the gap region. The incident ***E***-field ($\theta = \pi/4$) that drives the ***H***-field-generating displacement currents in the high refractive index Si nanoparticles also has a component along the long dimer axis in both nanoparticles, resulting in a strong simultaneous localization of ***E***-field intensity in the gap region of the dimer (**Figure 1c,** top). We conclude that the silicon nanodisk dimers achieve a parallel alignment of ***E***- and ***H***-fields and a significant enhancement of the respective field intensities in the gap region if excited with an off-axis incident ***E***-field. Electromagnetic interactions between Si nanodisks shift the MD resonance.[39,47] For instance, in a dimer with g = 20 nm the simulated MD resonance peaks at 579 nm (as shown in **Figure S1b** of the Supporting Information), compared to 563 nm in the monomer. Throughout the manuscript we analyzed the MD resonance at the peak wavelength of the Si nanodisk dimers unless otherwise noted. Gold nanodisk dimer benchmarks were evaluated at their respective ED resonance.

The colocalization and correct alignment of ***E***- and ***H***-fields is one requirement for near-field chirality enhancement, a second one is a non-zero phase difference between ***E*** and ***H***. Importantly, the phases of the ***E***- and ***H***-fields around a Si nanoparticle can have a significant difference.[29,53] This is illustrated in **Figure 1d** by plotting the simulated phase of the x-components of the ***E***-field (E_x) and ***H***-field (H_x) evaluated for one spot in the evanescent field of a D = 140 nm, h = 100 nm nanodisk excited with with a polarization of $\theta = \pi/4$. A non-zero phase shift between electric and magnetic field components within the envelope of the magnetic dipole resonance implies that the parallel ***E***- and ***H***-field components in the gap region of the Si nanodisk dimer will result in a net enhancement of the near-field chirality according to the definition of C. The top panel of **Figure 1e** shows a spatial map of the FDTD-simulated chirality density enhancement, C/C_0, where C_0 is the optical chirality of CPL, for a Si nanodisk dimer with a gap separation of g = 20 nm in the xy-plane and for an incident ***E***-field pointing at an angle of $\theta = \pi/4$. The map confirms a strong enhancement of C in the gap between the nanodisks. Importantly, the chirality density hot-spot formed between the nanodisks for an incident ***E***-field pointing in the direction of $\theta = \pi/4$ has a uniform sign, so that the dimer would selectively enhance the light absorption from one enantiomer. Interestingly, by rotating the incident polarization by $\pi/2$ from for $\theta = \pi/4$ to $\theta = ¾\ \pi$, the sign of C in the hot-spot can be inverted, allowing an enhancement of absorption from the other enantiomer simply by rotating the polarization of the incident linear light (**Figure 1e**, bottom). C/C_0 maps for additional polarization angles θ, as well as a summary plot of the peak value of C/C_0 as function of θ are included in **Figure S2** of the Supporting Information. These data confirm that off-axis components of the incident light polarization result in a θ-dependent, uniform sign chirality enhancement in the dimer gap region**.** We mention in passing that incident light with polarizations of $\theta = \pi/2$, and 0 (perpendicular and parallel to the long dimer axis) also generate regions of enhanced near-field chirality (albeit with lower peak enhancement than for θ

= π/4, ¾ π), but importantly these areas are generated in pairs of opposite sign so that the net enhancement is zero (**Figure 1f**).

Gap Dependence of Chirality Enhancement in Au and Si Nanodisk Dimers. Si nanodisk dimers increase the optical near-field chirality through enhancement of both ***E***- and ***H***-fields, whereas in plasmonic NP dimers the C/C_0 enhancement is determined by the ***E***-field enhancement through the NP dimer and its interaction with the incident ***H***-field. To allow a more quantitative comparison between the chirality density enhancement in Au and Si nanodisk dimers, we computed C/C_0 as function of the edge-to-edge interparticle separation, *g*, between *D* = 100 nm Au and *D* = 140 nm Si nanodisk dimers with height of 100 nm. The gold diameter was chosen to provide a spectrum that overlaps with that of the Si nanodisk dimers. In all cases the incident ***E***-field points in the direction of θ = π/4. We chose a *g*-range between 20 – 100 nm, which is experimentally accessible for both types of nanodisks through established top-down fabrication. The C/C_0 values were averaged over a square with side length of *g* centered in the dimer gap at a height of 50 nm. The resulting C/C_0 values (**Figure 2a**) are significantly higher for Si than for Au nanodisk dimers. For Si nanodisk dimers the computed C/C_0 values lie between 4-19 in the investigated *g*-range, which compares with 1-2.5 for the Au nanodisk dimers. A separate analysis of the ***E***-field and ***H***-field contributions (**Figure 2b**) shows that the ***E***-field intensity in the monitored gap range is almost identical for Si and Au nanodisk dimers. The ***H***-field intensity is, however 2-5 orders of magnitude higher for the Si nanodisk dimers. This analysis confirms that the significant difference in C/C_0 between the Au and Si nanodisk dimers arises from the enhancement of the magnetic field provided by the magnetic dipole resonance in the Si nanodisk dimer. Importantly, an increase in Au nanodisk diameter to the same size as the Si nanodisks (*D* = 140 nm) did not

increase C/C_0 but, instead, resulted in a decrease of C/C_0 due to stronger radiative losses in the larger metal NPs.

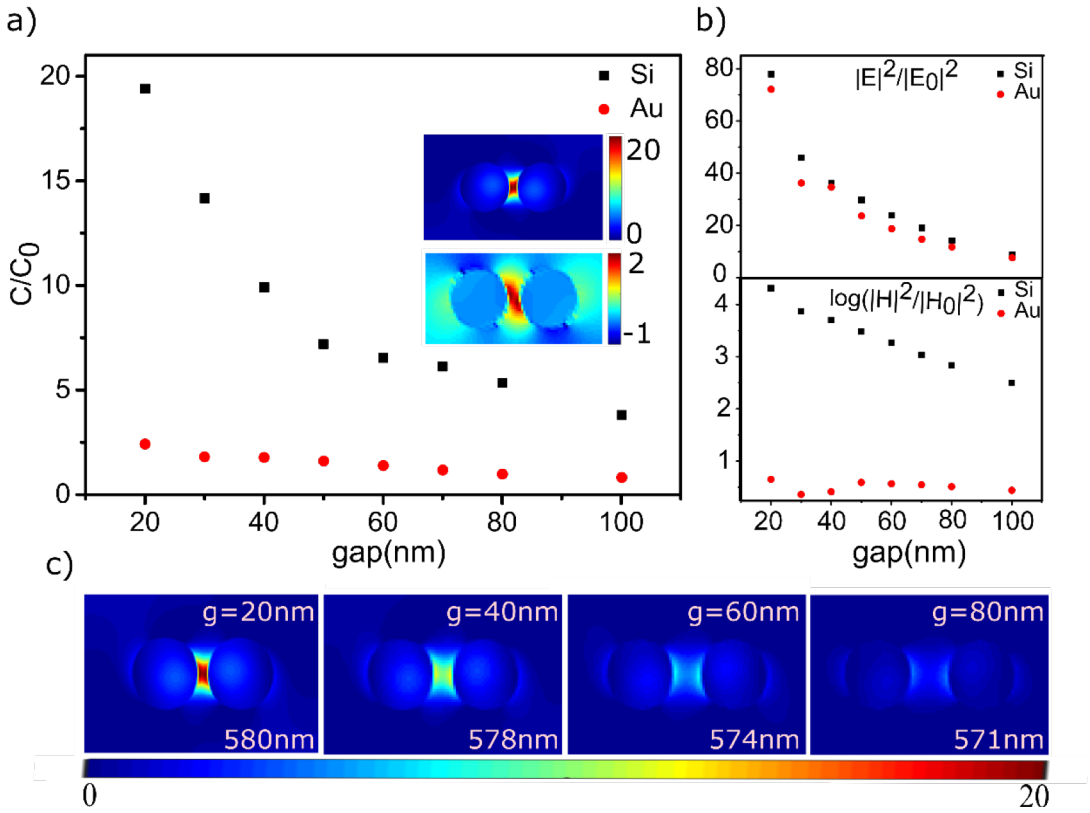

Figure 2. a) Optical chirality enhancement (C/C_0) for D = 140 nm, h = 100 nm Si nanodisk dimer (black square) and D = 100 nm, h = 100 nm diameter Au nanodisk dimer (red circle) as function of gap width, g. The C/C_0 values were obtained by averaging over a square with side-length g centered in the gap. Inset: chirality density maps for Si dimer (upper) and Au dimer (lower) with g = 20 nm. b) ***E***-field intensity enhancement (upper) and ***H***-field intensity enhancement (lower) for Si dimer (black square) and Au nanodisk dimer (red circle). The field intensities were obtained by averaging over a square with side-length g centered in the gap. c) Maps of optical chirality density enhancement, C/C_0, in the xy-plane for Si nanodisk dimers with different gap widths between g = 20 – 80 nm at the specified wavelengths. All simulations in this figure were performed with an incident polarization of θ = π/4.

Maps of the chirality density enhancement, C/C_0, in the Si nanodisk dimers with different inter-particle separations at the magnetic dipole resonance in **Figure 2c** show the evolution of the same-sign chirality density hot-spot in the gap region. It is clear from the maps that even at separations as large as g = 40 nm the entire gap region provides a significant enhancement of the chirality density. Compared to the length scales of typical molecules, 40 nm is very large. The ability to generate same-sign C enhancement in relatively large volumes is highly beneficial for

potential applications. We acknowledge that shorter interparticle separations than considered here will strongly enhance the near-field coupling between the plasmonic gold nanodisks, and that this increase will improve the C/C_0 ratio for the plasmonic antenna. However, a decrease in the gap below 20 nm requires higher precision fabrication and, importantly, reduces the accessible volume with enhanced near-field chirality.

Effect of the Substrate on Chirality Enhancement in Si Nanodisk Dimers. Our electromagnetic analysis so far focused on illustrating the fundamental working principles underlying chirality density enhancement in dimers of Si nanodisks with a height of 100 nm in vacuum. Next, we investigate the effect of the substrate and determine the ideal height of the Si nanodisks that optimizes chirality density enhancement in the presence of a sapphire substrate. The height of the disks is an important design criterion as only heights above a certain minimum threshold are able to support displacement currents in the xz und yz-planes required for magnetic dipoles.[30] Furthermore, modes in Si nanodisks supported by a substrate leak out of the resonator into the substrate with an efficiency that depends on the refractive index of the latter.[30,55] This effect is expected to weaken the electromagnetic interactions between the nanodisks that form the fundament of the C/C_0 enhancement in Si nanodisk dimers. In **Figure 3** we analyze the effect of a transparent sapphire substrate (n = 1.8) on the scattering spectra, mode volume, and chirality enhancement of D = 140 nm Si nanodisk dimers with heights of h_1 = 100 nm and h_2 = 150 nm. The simulated scattering spectra (**Figure 3a**) contain hypothetical "floating" nanodisk dimers (n = 1) for comparison. Both h_1 (left panel) and h_2 (right panel) dimers show a red-shift and broadening of the electric and magnetic dipole resonance relative to the n = 1 reference, indicative of an increased effective refractive medium, but the effects are stronger for h_1. The observed spectral differences are a first indication that the electric and magnetic dipole resonances of the higher nanodisks are less affected by the substrate.

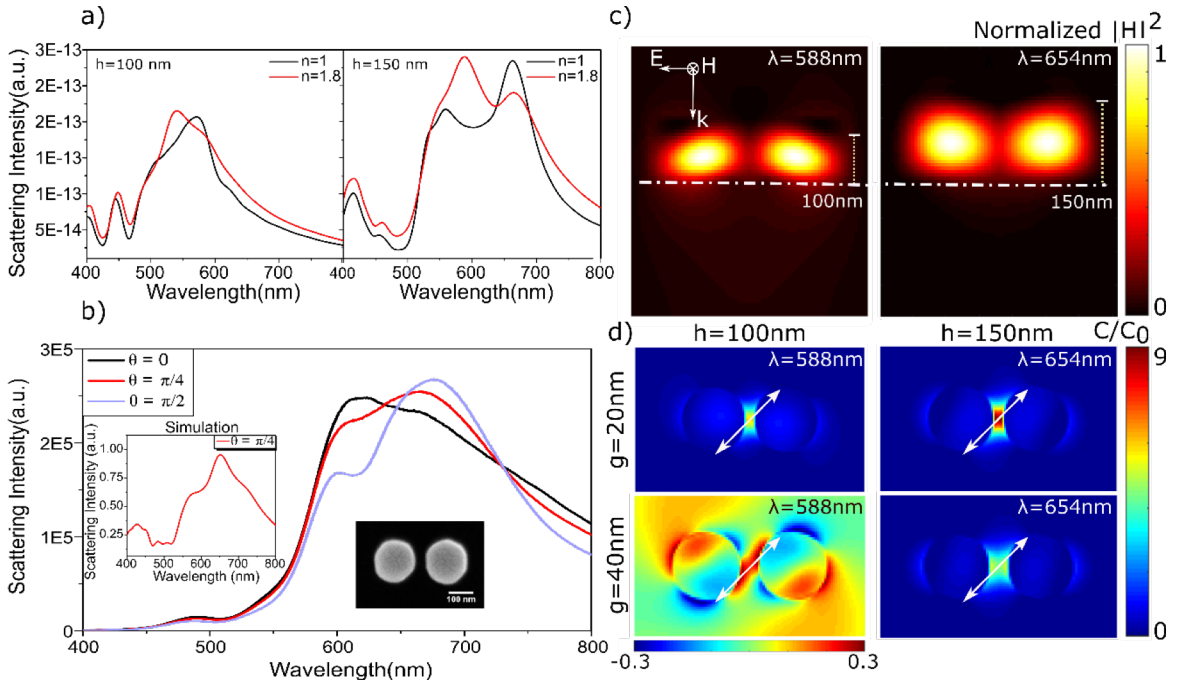

Figure 3. a) Simulated scattering spectra of silicon nanodisk dimers (D = 140 nm, g = 20 nm) with incident polarization of θ = π/4 with a height of h_1 = 100 nm (left) and h_2 = 150 nm (right) in air (black) and on sapphire substrate (red). b) Experimental scattering spectra of silicon nanodisk dimer (SEM image shown in the inset) (D = 160 nm, g = 40 nm) with h = 150 nm on sapphire substrate. The corresponding simulated scattering spectrum with incident polarization of θ = π/4 is shown in the inset. c) Simulated ***H***-field intensity map at MD resonances in the xz-plane. The air-substrate interfaces are indicated with white dash-dotted lines. d) Maps of the chirality density enhancement, C/C_0, in silicon nanodisk dimers for h_1 = 100 nm (left) and h_2 = 150 nm (right) and gap sizes of 20 nm (top) and 40 nm (bottom) at their respective MD resonance. The xy-plane is shown at a height of 50 nm (left) and 75 nm (right).

Experimental scattering spectra for the Si nanodisk dimer with D = 160 nm and height h = 150 nm are included in **Figure 3b** for incident light polarizations of θ = 0, π/2, π/4. The experimental spectrum with θ = π/2 shows a dominating magnetic dipole resonance and a shorter wavelength, lower intensity electric dipole resonance. If the incident light polarization points along the long dimer axis (θ = 0), the electric dipole resonance dominates as only the excited electric dipoles have the correct alignment to couple along the long axis of the dimer, while the overlap for the magnetic dipoles is poor. If the dimer is excited with an off-axis polarization (θ = π/4), the magnetic dipoles have a component along the long dimer axis required for coupling, and the magnetic dipole mode dominates again.

The simulated magnetic field intensity maps in **Figure 3c** illustrate the effect of the difference in Si nanodisk dimer height (h_1 versus h_2) on the mode volume of the magnetic dipole. For the shorter nanodisk height h_1 (left panel) the mode visibly leaks into the substrate, whereas for h_2 (right panel) the magnetic field is localized above the substrate and spatially well separated. The different degrees of field containment result in different levels of chirality density enhancement in Si nanodisk dimers. The spatial C/C_0 maps for sapphire supported dimers (D = 140, g = 20 nm) closely resembles those in vacuum (**Figure 1e**), but the peak chirality density enhancement has dropped to 6 (h_1 = 100 nm) and 9 (h_2 = 150 nm) when compared to 20 (h_1) and 13 (h_2) in vacuum. For the g = 40 nm dimer (**Figure 3d,** bottom row) the chirality density enhancement drops further, but importantly the h_2 dimer still achieves a uniform sign enhancement by a factor of 5 throughout the gap region under linearly polarized light excitation. We validated in test simulations that near-field chirality enhancement around the Si nanodisk dimers was observed for light incident from both the substrate or superstratum side.

Unlike in the simulation where the height of the nanodisks can be precisely controlled, in the experiments the height of nanodisks is less precisely defined. Different batches of Si nanodisks generated by reactive ion etching in this work show some variations in height. Although typical variations on the order of +/- 5 nm lead to small differences in the spectra of nanodisks and their dimers, for Si nanodisks with sufficient height to support magnetic dipole resonances height variations of this magnitude lead to negligible differences in optical chirality enhancement. This is shown in **Figure S3** of the Supporting Information.

Experimental Validation of Switchable Chiroptical Hot-Spots in Achiral Si Nanoparticle Dimers. Poulikakos *et al.* have introduced the optical chirality flux defined as $\boldsymbol{\mathcal{F}} = \frac{1}{4}[\boldsymbol{\mathcal{E}}\times(\nabla\times\boldsymbol{\mathcal{H}}^*) - \boldsymbol{\mathcal{H}}^*\times(\nabla\times\boldsymbol{\mathcal{E}})]$, where $\boldsymbol{\mathcal{E}}, \boldsymbol{\mathcal{H}}$ are the complex time-harmonic ***E***- and ***H***-fields, as a far-

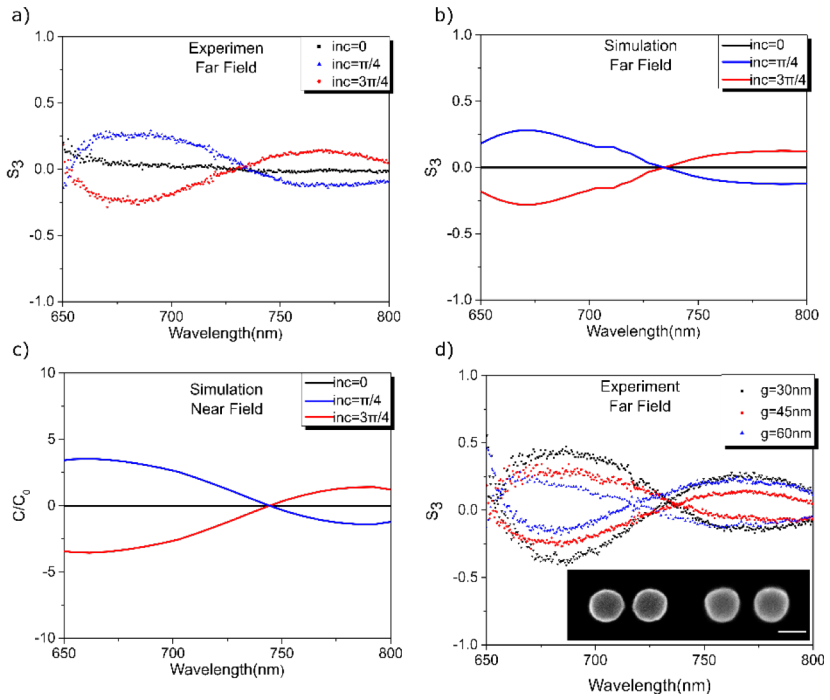

Figure 4. Comparison of experimental and simulated chiral optical response of a silicon nanodisk dimer with a diameter of *D* = 160 nm, separation of *g* = 40 nm, and height of h = 150 nm. a) Experimental third Stokes parameter, S_3, as function of wavelength with incident polarizations pointing in the following directions: θ = 0 (black), π/4 (red) and ¾ π (blue). b) Simulated S_3 spectra with the same linear light polarizations as in (a). c) Simulated optical chirality density enhancement (C/C_0) versus wavelength. d) Experimental S_3 spectra for dimers with different gap widths, *g*. Inset: SEM images of fabricated dimers with different *g* values. Scale bar = 100 nm.

field probe of chiral near-fields that is directly proportional to the third Stokes parameter, S_3.[56,57] Since linearly polarized light is a sum of two left and right CPL component of equal magnitude and phase, its net chirality flux is zero. If this linearly polarized light interacts, however, with a nanostructure, such as the Si nanodisk dimers described above, which generates a chiral near-field of one specific sign (handedness) through alignment of ***E***- and ***H***-fields, one handedness will be attenuated due to preferential dissipation in the structure. According to the conservation law of optical chirality as discussed by Poulikakos *et al.*, a nonzero chirality flux must then be generated which results in a nonzero S_3. In addition to the obvious advantage of facilitating

detection of near-field chirality in the far-field, measurements of S_3 do not require any labels and are applicable to any wavelength range. To characterize the chirality enhancement generated through the alignment of ***E***- and ***H***-fields associated with the magnetic dipole resonance, we measured S_3 in the wavelength range between 650 – 800 nm for D = 160 nm Si nanodisk dimers with g = 40 nm whose magnetic dipole resonance peaks at ~690 nm (**Figure 3b**). **Figure 4a** shows experimental S_3 spectra for Si nanodimers (D = 160 nm, g = 40 nm, h = 150 nm) with incident polarizations of $\theta = \pi/4$ (red) and $¾\ \pi$ (blue), respectively, in the wavelength range 650 – 800 nm. The control case with an incident polarization of $\theta = 0$ (parallel to long dimer axis) is included in black and is essentially zero at all wavelengths. In contrast, $\theta = \pi/4$ and $¾\ \pi$ result in distinct non-zero, wavelength-dependent S_3 values, confirming chiral near-field generation in the Si nanodisk dimer, provided the incident linear light polarization contains an off-axis component. The S_3 spectra for $\theta = \pi/4$ and $¾\ \pi$ have almost identical shapes but opposite sign, which is an experimental verification that the sign of the near-field chirality in the Si nanodisk dimers can be inverted by rotation of the incident linear light polarization. The measured S_3 spectra are also in excellent agreement with predicted third Stokes parameter provided by FDTD simulations (**Figure 4b**). In **Figure 4c** we plot the simulated optical chirality density enhancement (C/C_0) in the gap of the Si nanodimer as a function of wavelength. The shape and relative magnitude of the calculated near-field chirality enhancement is in overall good agreement with the experimental and simulated S_3 values, validating the value of the chirality flux as a far-field probe for near-field optical chirality. We conclude that electromagnetic simulations of the near-field chirality and far-field chirality flux, and experimental measurements of S_3 all independently confirm the direction of the incident light polarization as control parameter for the near-field chirality in the chiral hot-spots.

Fabrication imperfections and losses in the Si in the visible lead to relatively broad spectral features of the investigated nanodisks (**Figure 3b**). We anticipate that the spectral width of the C/C_0 can be sharpened by shifting the spectral response to wavelengths at which the Si

absorption is lower. A reduction in dissipative losses also allows for a further increase in the peak optical chirality enhancement (**Figure S4** of the Supporting Information). It is, however, also important to note that some dissipation is required to characterize the near-field chirality via the chirality flux in the far-field.

To further prove that the experimentally observed S_3 is generated through electromagnetic coupling of the Si nanodisks, we measured the effect of increasing gap separation (**Figure 4d**). These measurements revealed a clear gap-dependence of the measured S_3 values. In excellent agreement with our simulations of the near-field chirality in **Figure 3c**, we experimentally observed the amplitude of S_3 to drop with decreasing overlap of ***E***- and ***H***-fields as g is increased.

Conclusion

In this manuscript we have investigated the creation of same-sign near-field chirality in Si nanodisk dimers that are excited by linearly polarized light. Unlike noble metal nanoparticles that sustain only electric dipole plasmon resonances, high refractive index nanoparticles provide both electric and magnetic dipole resonances in the visible range of the electromagnetic spectrum. We have found that the magnetic resonance is of particular interest for enhancing optical chirality in assemblies of Si nanodisks. Optical excitation of the magnetic dipole resonance of an individual Si nanodisk generates enhanced ***E***- and ***H***-fields in the ambient space around the nanodisk that are stronger and penetrate deeper into the environment than is the case for the electric dipole resonance. Dimers of near-field coupled Si nanodisks achieve a further enhancement of ***E***- and ***H***-fields and, equally important, allow for an alignment of the enhanced ***E***- and ***H***-fields to achieve uniform-sign optical chirality density enhancement. Specifically, we demonstrated through FDTD simulations that excitation of the magnetic dipole resonances in two adjacent Si nanodisks by normally incident, linearly polarized light whose polarization points in the direction of $\theta = \pi/4$ (relative to the long dimer axis) results in the co-localization of enhanced and phase-shifted ***E***-

and ***H***-fields in the gap region. The simultaneous presence of ***E***- and ***H***-fields with a non-trivial phase shift within the entire envelope of the magnetic dipole resonance, results in the formation of chiroptical hot-spots in the dimer gap. The availability of enhanced ***E***- and ***H***-fields in case of the Si nanodisks results in a substantially higher near-field enhancement than for Au nanoparticle dimers whose plasmons overlap with the Si nanodisk dimer spectra in the investigated distance range $g > 20$ nm. We verified the results of the electromagnetic simulations through experimental analysis of the chirality flux, which is a the far-field probe of the near-field chirality generated in nanoantennas. Measurements of the third Stokes parameter, S_3, which is directly proportional to the chirality flux, confirmed the generation of optical chirality density in Si nanodisk dimers under illumination with linearly polarized light whose polarization was pointing in the direction of $\theta = \pi/4$. In excellent agreement with electromagnetic simulations, a rotation of the incident polarization by $\pi/2$ to $\theta = ¾\ \pi$ resulted in the inversion of the sign of the S_3, indicating a change in the handedness of the associated near-field chirality.

The ability to generate hot-spots of enhanced electromagnetic fields and same-sign optical chirality of defined handedness in achiral Si nanodisks using linearly polarized light as demonstrated in this manuscript paves the path to new surface-enhanced chiroptical spectroscopies with greatly enhanced sensitivities. Rationally designed Si nanoantennas with optimized chiral hot-spots can contribute to overcome key limitations of current chiroptical spectroscopies, such as the need for high concentrations and long acquisition times, in the future.

Acknowledgement

This work was partly financially supported by the National Science Foundation through grants CHE-1609778 and CHE-1808241. Some fabrication was performed at the Center for Nanoscale Systems (CNS) at Harvard University, which is supported by the National Science Foundation through grant ECS 1541959.

Supporting Information

Scattering spectra of individual nanodisks with diameters D = 140 nm, 160 nm, 180nm. Simulated scattering spectra for nanodisk dimer for different directions of linear polarization. Optical chirality enhancement as function of linear light polarization. Effect of fabrication inaccuracy on C/C_0. Optical chirality enhancement for Si nanodisk dimers without imaginary component of refractive index.

References

(1) Fischer, E. Ueber Die Configuration Des Traubenzuckers Und Seiner Isomeren. II. *Berichte der Dtsch. Chem. Gesellschaft* **1891**, *24* (2), 2683–2687.

(2) Tokunaga, E.; Yamamoto, T.; Ito, E.; Shibata, N. Understanding the Thalidomide Chirality in Biological Processes by the Self-Disproportionation of Enantiomers. *Sci. Rep.* **2018**, *8* (1), 17131. https://doi.org/10.1038/s41598-018-35457-6.

(3) Nguyen, L. A.; He, H.; Pham-Huy, C. Chiral Drugs: An Overview. *Int. J. Biomed. Sci.* **2006**, *2* (2), 85–100.

(4) Tang, Y.; Cohen, A. E. Optical Chirality and Its Interaction with Matter. *Phys. Rev. Lett.* **2010**, *104* (16), 163901.

(5) Greenfield, N. J. Using Circular Dichroism Spectra to Estimate Protein Secondary Structure. *Nat. Protoc.* **2007**, *1*, 2876.

(6) Stephens, P. J.; Lowe, M. A. Vibrational Circular Dichroism. *Annu. Rev. Phys. Chem.* **1985**, *36* (1), 213–241. https://doi.org/10.1146/annurev.pc.36.100185.001241.

(7) Hendry, E.; Carpy, T.; Johnston, J.; Popland, M.; Mikhaylovskiy, R. V; Lapthorn, A. J.; Kelly, S. M.; Barron, L. D.; Gadegaard, N.; Kadodwala, M. Ultrasensitive Detection and Characterization of Biomolecules Using Superchiral Fields. *Nat. Nanotechnol.* **2010**, *5* (11), 783–787.

(8) Lipkin, D. M. Existence of a New Conservation Law in Electromagnetic Theory. *J. Math. Phys.* **1964**, *5* (5), 696–700.

(9) Tian, X.; Fang, Y.; Sun, M. Formation of Enhanced Uniform Chiral Fields in Symmetric Dimer Nanostructures. *Sci. Rep.* **2015**, *5*, 17534. https://doi.org/10.1038/srep17534.

(10) Schäferling, M.; Yin, X.; Engheta, N.; Giessen, H. Helical Plasmonic Nanostructures as Prototypical Chiral Near-Field Sources. *ACS Photonics* **2014**, *1* (6), 530–537. https://doi.org/10.1021/ph5000743.

(11) Tang, Y.; Sun, L.; Cohen, A. E. Chiroptical Hot Spots in Twisted Nanowire Plasmonic Oscillators. *Appl. Phys. Lett.* **2013**, *102* (4), 43103. https://doi.org/10.1063/1.4789529.

(12) Schäferling, M.; Dregely, D.; Hentschel, M.; Giessen, H. Tailoring Enhanced Optical Chirality: Design Principles for Chiral Plasmonic Nanostructures. *Phys. Rev. X* **2012**, *2* (3), 31010.

(13) Meinzer, N.; Hendry, E.; Barnes, W. L. Probing the Chiral Nature of Electromagnetic Fields Surrounding Plasmonic Nanostructures. *Phys. Rev. B - Condens. Matter Mater. Phys.* **2013**, *88* (4), 1–5. https://doi.org/10.1103/PhysRevB.88.041407.

(14) Hentschel, M.; Schäferling, M.; Duan, X.; Giessen, H.; Liu, N. Chiral Plasmonics. *Sci. Adv.* **2017**, *3* (5), e1602735. https://doi.org/10.1126/sciadv.1602735.

(15) Schäferling, M.; Engheta, N.; Giessen, H.; Weiss, T. Reducing the Complexity: Enantioselective Chiral Near-Fields by Diagonal Slit and Mirror Configuration. *ACS Photonics* **2016**, *3* (6), 1076–1084. https://doi.org/10.1021/acsphotonics.6b00147.

(16) Hendry, E.; Mikhaylovskiy, R. V; Barron, L. D.; Kadodwala, M.; Davis, T. J. Chiral Electromagnetic Fields Generated by Arrays of Nanoslits. *Nano Lett.* **2012**, *12* (7), 3640–3644. https://doi.org/10.1021/nl3012787.

(17) Esposito, M.; Tasco, V.; Cuscunà, M.; Todisco, F.; Benedetti, A.; Tarantini, I.; Giorgi, M. De; Sanvitto, D.; Passaseo, A. Nanoscale 3D Chiral Plasmonic Helices with Circular

Dichroism at Visible Frequencies. *ACS Photonics* **2015**, *2* (1), 105–114. https://doi.org/10.1021/ph500318p.

(18) Ferry, V. E.; Hentschel, M.; Alivisatos, A. P. Circular Dichroism in Off-Resonantly Coupled Plasmonic Nanosystems. *Nano Lett.* **2015**, *15* (12), 8336–8341. https://doi.org/10.1021/acs.nanolett.5b03970.

(19) Govorov, A. O.; Fan, Z.; Hernandez, P.; Slocik, J. M.; Naik, R. R. Theory of Circular Dichroism of Nanomaterials Comprising Chiral Molecules and Nanocrystals: Plasmon Enhancement, Dipole Interactions, and Dielectric Effects. *Nano Lett.* **2010**, *10* (4), 1374–1382. https://doi.org/10.1021/nl100010v.

(20) Alizadeh, M. H.; Reinhard, B. M. Plasmonically Enhanced Chiral Optical Fields and Forces in Achiral Split Ring Resonators. *ACS Photonics* **2015**, *2* (3), 361–368. https://doi.org/10.1021/ph500399k.

(21) Schäferling, M.; Yin, X.; Giessen, H. Formation of Chiral Fields in a Symmetric Environment. *Opt. Express* **2012**, *20* (24), 26326–26336. https://doi.org/10.1364/OE.20.026326.

(22) Biagioni, P.; Savoini, M.; Huang, J.-S.; Duò, L.; Finazzi, M.; Hecht, B. Near-Field Polarization Shaping by a near-Resonant Plasmonic Cross Antenna. *Phys. Rev. B* **2009**, *80* (15), 153409. https://doi.org/10.1103/PhysRevB.80.153409.

(23) Decker, M.; Staude, I.; Falkner, M.; Dominguez, J.; Neshev, D. N.; Brener, I.; Pertsch, T.; Kivshar, Y. S. High-Efficiency Dielectric Huygens' Surfaces. *Adv. Opt. Mater.* **2015**, *3* (6), 813–820. https://doi.org/10.1002/adom.201400584.

(24) Shibanuma, T.; Albella, P.; Maier, S. A. Unidirectional Light Scattering with High Efficiency at Optical Frequencies Based on Low-Loss Dielectric Nanoantennas. *Nanoscale* **2016**, *8* (29), 14184–14192. https://doi.org/10.1039/C6NR04335F.

(25) Yan, J. H.; Liu, P.; Lin, Z. Y.; Wang, H.; Chen, H. J.; Wang, C. X.; Yang, G. W.

Magnetically Induced Forward Scattering at Visible Wavelengths in Silicon Nanosphere Oligomers. *Nat. Commun.* **2015**, *6*, 7042.

(26) Kuznetsov, A. I.; Miroshnichenko, A. E.; Brongersma, M. L.; Kivshar, Y. S.; Luk\textquoterightyanchuk, B. Optically Resonant Dielectric Nanostructures. *Science (80-.).* **2016**, *354* (6314). https://doi.org/10.1126/science.aag2472.

(27) Zhou, Z.; Li, J.; Su, R.; Yao, B.; Fang, H.; Li, K.; Zhou, L.; Liu, J.; Stellinga, D.; Reardon, C. P.; et al. Efficient Silicon Metasurfaces for Visible Light. *ACS Photonics* **2017**, *4* (3), 544–551. https://doi.org/10.1021/acsphotonics.6b00740.

(28) Malekfar, M. R.; Shokooh-Saremi, M.; Mirsalehi, M. M. Design of Highly Transmissive All-Dielectric Metasurface Based on Silicon Nanodisks. *Photonics Nanostructures - Fundam. Appl.* **2018**, *31*, 140–146. https://doi.org/10.1016/J.PHOTONICS.2018.07.002.

(29) García-Etxarri, A.; Dionne, J. A. Surface-Enhanced Circular Dichroism Spectroscopy Mediated by Nonchiral Nanoantennas. *Phys. Rev. B - Condens. Matter Mater. Phys.* **2013**, *87* (23), 1–5. https://doi.org/10.1103/PhysRevB.87.235409.

(30) Groep, J. Van De; Polman, a. Designing Dielectric Resonators on Substrates : Combining Magnetic and Electric Resonances. *Opt. Express* **2013**, *21* (22), 1253–1257. https://doi.org/10.1364/OE.21.026285.

(31) Bakker, R. M.; Permyakov, D.; Yu, Y. F.; Markovich, D.; Paniagua-Domínguez, R.; Gonzaga, L.; Samusev, A.; Kivshar, Y.; Lukyanchuk, B.; Kuznetsov, A. I. Magnetic and Electric Hotspots with Silicon Nanodimers. *Nano Lett.* **2015**, *15* (3), 2137–2142. https://doi.org/10.1021/acs.nanolett.5b00128.

(32) Zywietz, U.; Evlyukhin, A. B.; Reinhardt, C.; Chichkov, B. N. Laser Printing of Silicon Nanoparticles with Resonant Optical Electric and Magnetic Responses. *Nat. Commun.* **2014**, *5*, 3402.

(33) Butet, J.; Martin, O. J. F. Tailoring the Field Enhancement in Fano-Resonant

Nanoantennas for Improved Optical Bistability. *J. Nanophotonics* **2017**, *11* (1), 16007.

(34) Staude, I.; Miroshnichenko, A. E.; Decker, M.; Fofang, N. T.; Liu, S.; Gonzales, E.; Dominguez, J.; Luk, T. S.; Neshev, D. N.; Brener, I.; et al. Tailoring Directional Scattering through Magnetic and Electric Resonances in Subwavelength Silicon Nanodisks. *ACS Nano* **2013**, *7* (9), 7824–7832. https://doi.org/10.1021/nn402736f.

(35) Kuznetsov, A. I.; Miroshnichenko, A. E.; Fu, Y. H.; Zhang, J.; Luk'yanchuk, B. Magnetic Light. *Sci. Rep.* **2012**, *2*, 492.

(36) Butakov, N. A.; Schuller, J. A. Designing Multipolar Resonances in Dielectric Metamaterials. *Sci. Rep.* **2016**, *6*, 38487.

(37) Evlyukhin, A. B.; Reinhardt, C.; Chichkov, B. N. Multipole Light Scattering by Nonspherical Nanoparticles in the Discrete Dipole Approximation. *Phys. Rev. B* **2011**, *84* (23), 235429. https://doi.org/10.1103/PhysRevB.84.235429.

(38) Solomon, M. L.; Hu, J.; Lawrence, M.; García-Etxarri, A.; Dionne, J. A. Enantiospecific Optical Enhancement of Chiral Sensing and Separation with Dielectric Metasurfaces. *ACS Photonics* **2019**, *6* (1), 43–49. https://doi.org/10.1021/acsphotonics.8b01365.

(39) Zywietz, U.; Schmidt, M. K.; Evlyukhin, A. B.; Reinhardt, C.; Aizpurua, J.; Chichkov, B. N. Electromagnetic Resonances of Silicon Nanoparticle Dimers in the Visible. *ACS Photonics* **2015**, *2* (7), 913–920. https://doi.org/10.1021/acsphotonics.5b00105.

(40) van de Groep, J.; Coenen, T.; Mann, S. A.; Polman, A. Direct Imaging of Hybridized Eigenmodes in Coupled Silicon Nanoparticles. *Optica* **2016**, *3* (1), 93–99. https://doi.org/10.1364/OPTICA.3.000093.

(41) Yao, K.; Liu, Y. Enhancing Circular Dichroism by Chiral Hotspots in Silicon Nanocube Dimers. *Nanoscale* **2018**, *10* (18), 8779–8786. https://doi.org/10.1039/C8NR00902C.

(42) Zhang, W.; Wu, T.; Wang, R.; Zhang, X. Amplification of the Molecular Chiroptical Effect by Low-Loss Dielectric Nanoantennas. *Nanoscale* **2017**, *9* (17), 5701–5707.

https://doi.org/10.1039/C7NR01527E.

(43) Reinhard, B. M.; Siu, M.; Agarwal, H.; Alivisatos, A. P.; Liphardt, J. Calibration of Dynamic Molecular Rulers Based on Plasmon Coupling between Gold Nanoparticles. *Nano Lett.* **2005**, *5* (11), 2246–2252. https://doi.org/10.1021/nl051592s.

(44) Su, K.-H.; Wei, Q.-H.; Zhang, X.; Mock, J. J.; Smith, D. R.; Schultz, S. Interparticle Coupling Effects on Plasmon Resonances of Nanogold Particles. *Nano Lett.* **2003**, *3* (8), 1087–1090. https://doi.org/10.1021/nl034197f.

(45) Prodan, E.; Radloff, C.; Halas, N. J.; Nordlander, P. A Hybridization Model for the Plasmon Response of Complex Nanostructures. *Science (80-.).* **2003**, *302* (5644), 419–422. https://doi.org/10.1126/science.1089171.

(46) Yan, B.; Boriskina, S. V; Reinhard, B. M. Design and Implementation of Noble Metal Nanoparticle Cluster Arrays for Plasmon Enhanced Biosensing. *J. Phys. Chem. C. Nanomater. Interfaces* **2011**, *115* (50), 24437–24453. https://doi.org/10.1021/jp207821t.

(47) Albella, P.; Poyli, M. A.; Schmidt, M. K.; Maier, S. A.; Moreno, F.; Sáenz, J. J.; Aizpurua, J. Low-Loss Electric and Magnetic Field-Enhanced Spectroscopy with Subwavelength Silicon Dimers. *J. Phys. Chem. C* **2013**, *117* (26), 13573–13584. https://doi.org/10.1021/jp4027018.

(48) Narushima, T.; Hashiyada, S.; Okamoto, H. Nanoscopic Study on Developing Optical Activity with Increasing Chirality for Two-Dimensional Metal Nanostructures. *ACS Photonics* **2014**, *1* (8), 732–738. https://doi.org/10.1021/ph500171t.

(49) Wu, X.; Xu, L.; Liu, L.; Ma, W.; Yin, H.; Kuang, H.; Wang, L.; Xu, C.; Kotov, N. A. Unexpected Chirality of Nanoparticle Dimers and Ultrasensitive Chiroplasmonic Bioanalysis. *J. Am. Chem. Soc.* **2013**, *135* (49), 18629–18636. https://doi.org/10.1021/ja4095445.

(50) Yang, S.-C.; Richter, K.; Fischer, W.-J. Multicolor Generation Using Silicon Nanodisk

Absorber. *Appl. Phys. Lett.* **2015**, *106* (8), 81112. https://doi.org/10.1063/1.4913847.

(51) Okhlopkov, K. I.; Ezhov, A. A.; Shafirin, P. A.; Shorokhov, A. S.; Orlikovsky, N. A.; Shcherbakov, M. R.; Fedyanin, A. A. Optical Coupling between Resonant Dielectric Nanoparticles and Dielectric Waveguides Probed by Third Harmonic Generation Microscopy. *J. Phys. Conf. Ser.* **2018**, *1092*, 12104. https://doi.org/10.1088/1742-6596/1092/1/012104.

(52) Fu, Y. H.; Kuznetsov, A. I.; Miroshnichenko, A. E.; Yu, Y. F.; Luk'yanchuk, B. Directional Visible Light Scattering by Silicon Nanoparticles. *Nat. Commun.* **2013**, *4*, 1527.

(53) García-Etxarri, A.; Gómez-Medina, R.; Froufe-Pérez, L. S.; López, C.; Chantada, L.; Scheffold, F.; Aizpurua, J.; Nieto-Vesperinas, M.; Sáenz, J. J. Strong Magnetic Response of Submicron Silicon Particles in the Infrared. *Opt. Express* **2011**, *19* (6), 4815–4826. https://doi.org/10.1364/OE.19.004815.

(54) Evlyukhin, A. B.; Novikov, S. M.; Zywietz, U.; Eriksen, R. L.; Reinhardt, C.; Bozhevolnyi, S. I.; Chichkov, B. N. Demonstration of Magnetic Dipole Resonances of Dielectric Nanospheres in the Visible Region. *Nano Lett.* **2012**, *12* (7), 3749–3755. https://doi.org/10.1021/nl301594s.

(55) Spinelli, P.; Verschuuren, M. A.; Polman, A. Broadband Omnidirectional Antireflection Coating Based on Subwavelength Surface Mie Resonators. *Nat. Commun.* **2012**, *3*, 692.

(56) Poulikakos, L. V; Gutsche, P.; McPeak, K. M.; Burger, S.; Niegemann, J.; Hafner, C.; Norris, D. J. Optical Chirality Flux as a Useful Far-Field Probe of Chiral Near Fields. *ACS Photonics* **2016**, *3* (9), 1619–1625. https://doi.org/10.1021/acsphotonics.6b00201.

(57) Poulikakos, L. V; Thureja, P.; Stollmann, A.; De Leo, E.; Norris, D. J. Chiral Light Design and Detection Inspired by Optical Antenna Theory. *Nano Lett.* **2018**, *18* (8), 4633–4640. https://doi.org/10.1021/acs.nanolett.8b00083.

For Table of Content use only

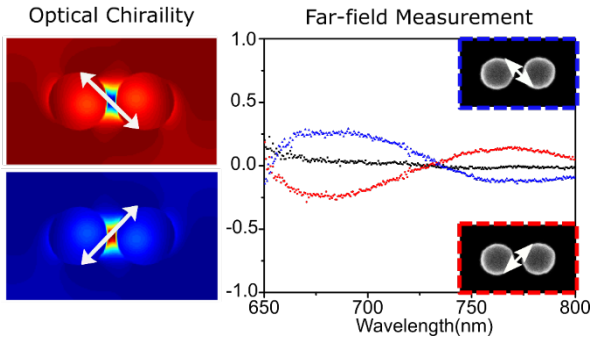

Switchable Chiroptical Hot-Spots in Silicon Nanodisk Dimers

Xin Zhao and Björn M. Reinhard

Synopsis: Optical chirality generation under linearly polarized light excitation in achiral silicon nanodisk dimers is investigated through far-field analysis of the optical chirality flux.